RESEARCH ARTICLE | OCTOBER 20 2025

High-quality photon-limited imaging through dynamic and complex scattering media with a single-photon detector

Special Collection: Single-photon detectors: new physical principles, circuits and applications

Yining Hao ; Yang Peng ; Tianshun Zhang ; Wen Chen

APL Photonics 10, 106119 (2025)
https://doi.org/10.1063/5.0293168

High-quality photon-limited imaging through dynamic and complex scattering media with a single-photon detector

Cite as: APL Photon. 10, 106119 (2025); doi: 10.1063/5.0293168
Submitted: 25 July 2025 • Accepted: 6 October 2025 •
Published Online: 20 October 2025

Yining Hao,[1] Yang Peng,[1] Tianshun Zhang,[1] and Wen Chen[1,2,a)]

AFFILIATIONS

[1] Department of Electrical and Electronic Engineering, The Hong Kong Polytechnic University, Hong Kong, China
[2] Photonics Research Institute, The Hong Kong Polytechnic University, Hong Kong, China

Note: This paper is part of the Special Topic on Single-photon detectors: new physical principles, circuits and applications.
[a)]**Author to whom correspondence should be addressed:** owen.chen@polyu.edu.hk

ABSTRACT

Recent advances in single-photon detectors have enabled low-light detection in diverse applications ranging from biological imaging to astronomy. However, it remains a challenge to realizing high-quality optical imaging through dynamic and complex scattering media under photon-limited conditions. In this paper, we report high-quality photon-limited imaging through dynamic and complex scattering media using a single-photon detector. To eliminate a series of dynamic scaling factors induced by complex scattering in dynamic media, an iterative algorithm is developed to retrieve an estimated object image and a series of corrected measurements, revealing a correlation relationship between the illumination patterns and corrected measurements. Then, the estimated object image and corrected measurements are fed to an untrained neural network powered by regularization with denoising for quality enhancement. Experimental results demonstrate that the proposed method can be applied to implement high-quality photon-limited imaging through complex scattering media at low-light levels. This work opens up an avenue for exploring photon-limited imaging in challenging environments with a single-photon detector.

I. INTRODUCTION

Imaging techniques usually require over 1000 photons per pixel to reconstruct a high-quality object image.[1–3] However, in many real-world scenarios, only a limited number of photons can be detected due to practical constraints, such as short detection time and low light. A single-photon detector has high sensitivity, which is capable of detecting individual photons of the light.[4–8] This superior capability makes it to be a suitable tool for applications under low-light conditions.[9–14] Although recent advances in single-photon detection and computational imaging enable object reconstruction with a few photons per pixel, it still remains a challenge to realizing photon-limited imaging through dynamic and complex scattering media.

Imaging through scattering media has been a fundamental problem across diverse fields. The light can be scattered into unpredictable paths, thus breaking the point-to-point mapping for image formation. To overcome this challenge, various methods have been developed. Wavefront shaping uses optical devices, such as spatial light modulator (SLM) or deformable mirrors, to adjust the incident light based on the measured deviations from ideal wavefront.[15–17] Other approaches to manipulating wave propagation through scattering media based on optical phase conjugation[18] and transmission matrix[19,20] were also developed. Moreover, optical memory effect[21] can be adopted to realize imaging through scattering media in a simple way. Despite the remarkable progress made in imaging through scattering media, low-light conditions can introduce a challenge to this problem, and few approaches have been explored.

Single-pixel imaging (SPI)[22] has emerged as an effective solution to imaging through scattering media. In SPI, a series of illumination patterns are displayed by SLM to modulate incident light, and the corresponding light intensities are recorded by a single-pixel detector without any spatial resolution. The object image can be reconstructed by a computational means.[23–26] Due to its

indirect approach, SPI has shown great potential in overcoming the challenges of imaging through scattering media.[27–29] To improve its imaging performance, much effort has been made to realize high-quality object reconstruction, such as SPI with compressive sensing[30,31] and deep learning.[32–34] However, the sequential recording nature inherently limits the performance of SPI in dynamic and complex scattering environments, where the measurements or realizations could be severely distorted by a series of dynamic scaling factors. Moreover, conventional photodetectors utilized in most SPI systems would be no longer effective under low-light conditions. It is desirable to advance object reconstruction algorithms and optical system designs to realize high-quality SPI through complex scattering media under low-light conditions.

In this paper, we report high-quality photon-limited imaging through complex scattering media with a single-photon detector. The SPI setup is established with a single-photon detector to enable imaging at low-light levels. An iterative algorithm is developed for object reconstruction, which incorporates scaling factors into a constraint on a series of intensity measurements. The designed algorithm is applied to correct wave distortions caused by complex scenarios while simultaneously estimating an effective object image. To enhance the imaging quality, the estimated object image and corrected measurements are fed to an untrained neural network powered by regularization with denoising (URED). Optical experiments are conducted in complex environments with low-light levels, and it is demonstrated that the proposed method can facilitate to achieve high-quality photon-limited imaging through complex scattering media at low-light levels.

II. METHODS

A. Object reconstruction

The measurement is performed in an SPI framework assisted by single-photon detection. The collected light intensity B corresponding to an illumination pattern can be described by

$$B_i = \left| \int\int P_i(x,y) O(x,y) dxdy \right|^2, \tag{1}$$

where $i = 1, 2, 3, \ldots, M, M$ denotes the total number of measurements (i.e., 2048 in this study), $P_i(x,y)$ denotes the ith random illumination pattern, and $O(x,y)$ denotes an object. Under photon-limited conditions, the light intensity can be derived from photon counts measured using a single-photon detector.[35]

When dynamic and complex scattering media exist in the optical channel, a series of dynamic or nonlinear scaling factors are induced. The measurements in complex media can be described by

$$\widehat{B}_i = \alpha_i B_i, \tag{2}$$

where $\widehat{B}_i$ denotes the ith distorted measurement and α_i denotes a scaling factor. The proposed method employs a scaling factor that generalizes the total distortion effect imposed on each single-pixel light intensity measurement. The reconstruction usually relies on the correlation between each illumination pattern and a corresponding measurement. However, with the presence of complex and dynamic scattering media, the scaling factors dynamically vary in the optical channel, and the inherent correlation property is broken by the series of time-varying scaling factors.

To reconstruct an object image from the series of distorted measurements, an iterative algorithm is designed here to correct the measurements while reconstructing an object image. The iterative procedure[29] adopts a strategy similar to Fienup's hybrid input–output algorithm.[36] In the designed iterative algorithm, the goal is to find an object image $f(x,y)$ such that

$$\widehat{B}_i \approx \alpha_i \left| \int\int P_i(x,y) f(x,y) dxdy \right|^2. \tag{3}$$

Equation (3) can be interpreted by using a zero-frequency component of the generated Fourier spectrum $G(\xi,\eta)$, as described by

$$\begin{aligned} G_i(\xi,\eta) &= FT[P_i(x,y) f(x,y)] \\ &= \iint P_i(x,y) f(x,y) e^{-j2\pi(\xi x+\eta y)} dxdy, \end{aligned} \tag{4}$$

where FT denotes Fourier transform and $j = \sqrt{-1}$. Here, Fourier transform is utilized to describe wave propagation between the object plane and the detection plane in the far field.

The proposed iterative algorithm starts with a random guess of $f_0(x,y)$, and the dynamic scaling factor α_i is initialized by using all-ones. For the ith illumination pattern $P_i(x,y)$, Fourier spectrum $G_i(\xi,\eta)$ is calculated and its zero-frequency component is replaced by the square root of a corresponding corrected measurement generated by dividing $\widehat{B}_i$ by α_i. The updated Fourier spectrum $G_i'(\xi,\eta)$ can be described by

$$G_i'(\xi,\eta) = \begin{cases} \sqrt{\dfrac{\widehat{B}_i}{\alpha_i}}, & (\xi,\eta) = (0,0), \\ G_i(\xi,\eta), & \text{Others.} \end{cases} \tag{5}$$

Then, inverse Fourier transform is performed on the updated Fourier spectrum to be projected back to the spatial domain. The resultant $g(x,y)$ can represent a product between an illumination pattern and the object pattern. Therefore, the object image can be updated by minimizing a distance between $g(x,y)$ and $P_i(x,y) f(x,y)$ as described by

$$\underset{f}{\operatorname{argmin}} \| g(x,y) - P_i(x,y) f(x,y) \|^2. \tag{6}$$

The above minimization problem can be solved using gradient descent, and an updated object image can be described by

$$f'(x,y) = f(x,y) + \beta P_i(x,y)[g(x,y) - P_i(x,y) f(x,y)], \tag{7}$$

where $f'(x,y)$ denotes an updated object image and β denotes a coefficient to control the convergence.

In terms of the next measurement (i.e., $i = i + 1$), $f'(x,y)$ is used to replace $f(x,y)$, and the above steps are repeated. One cycle is considered to be completed when all the measurements (i.e., $i = M$) are processed. After each cycle, the updated object image is denoted as $f_n(x,y)$ where n denotes the cycle number. Then, the series of dynamic scaling factors is updated as described by

$$\widehat{\alpha}_i = \frac{\widehat{B}_i}{\left| \iint P_i(x,y) f_n(x,y) dxdy \right|^2}. \tag{8}$$

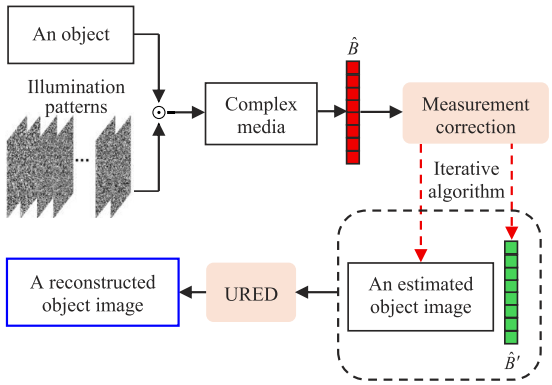

FIG. 1. A block diagram for the proposed photon-limited imaging through complex media: $\odot$, an element-wise product; $\widehat{B}$, a series of measurements (i.e., corresponding to the measured photon counts); and $\widehat{B}'$, a series of corrected data.

Furthermore, a wavelet denoiser[37] is applied to process the sequence of scaling factors. The cycle is repeated to process the measurements. Here, the convergence is satisfied when a mean squared error between $f_{n-1}(x,y)$ and $f_n(x,y)$ is smaller than a pre-defined threshold, i.e., 0.001. Finally, the proposed iterative algorithm can output an object image denoted as $\bar{f}(x,y)$ and a series of corrected data (measurements) $\widehat{B}' = \widehat{B}/\widehat{\alpha}$.

A block diagram for the proposed photon-limited imaging is shown in Fig. 1. The light modulated by random illumination pattern interacts with an object and passes through dynamic and complex scattering media. To eliminate wave distortions caused by complex scattering media, the proposed iterative algorithm is first applied to correct the distorted measurements. The proposed iterative algorithm can output an estimated object image and a series of corrected measurements to be further fed to a designed URED for quality enhancement.

B. The URED

An untrained neural network (UNN) with a physical model is further implemented for quality enhancement. The recovered object image $\bar{f}(x,y)$ obtained by using the proposed iterative algorithm is used as an input of the designed neural network. An objective function[34] of the designed UNN-based enhancement scheme can be described by

$$\min_{z,\theta}\left\{\frac{1}{2}\left\|H\left(U_\theta\left(\bar{f}\right)\right)-\widehat{B}'\right\|^2+\lambda\rho(z)\right\},\ \text{s.t.}\quad z=U_\theta\left(\bar{f}\right),\qquad(9)$$

where $H(\cdot)$ denotes a forward model in SPI, U_θ denotes the designed UNN with parameters θ, λ denotes a coefficient, $\rho(z)$ denotes a regularization term, and z denotes the UNN output.

Regularization by denoising is applied in the designed UNN with an explicit denoiser as a *prior*. However, a direct application of the denoiser would induce high complexity to the differentiation operation. Alternating directions of the multipliers (ADMM)[38] is a powerful algorithm that establishes a framework for incorporating different sub-problems. With ADMM, the data-fidelity term and regularization term in Eq. (9) can be separated to allow a parallel execution of the neural network and the denoiser. In this study, a non-local means (NLM)[39] is utilized as an explicit denoiser, and the NAFNet[40] is utilized as U_θ. The designed URED scheme is implemented on an NVIDIA GeForce RTX 4090 GPU, and the Adam optimizer with a learning rate of 0.001 is adopted to optimize parameters of the designed UNN.

III. RESULTS AND DISCUSSION

To verify the proposed photon-limited imaging in complex scenarios, experiments are conducted using an optical setup in Fig. 2. A green laser (MGL-III-532nm) with a wavelength of 532.0 nm and a maximum output power of 200.0 mW is used. The laser beam is expanded by an objective lens with a magnification factor of 40× and is collimated before illuminating SLM (Holoeye, HED 6001). A series of random illumination patterns are sequentially displayed by SLM. A 4*f* system is implemented to focus the reflected light onto an object, and a water tank is placed behind the object. The water tank has dimensions of 5.0 cm (length) × 10.0 cm (width) × 30.0 cm (height) and initially contains 1000 ml clean water. Skimmed milk diluted with 250.0 ml clean water is continuously dripped into the water tank in experiments, and a stirrer operating at 500 rpm is placed inside the water tank to create a dynamic and complex scattering environment. A fiber coupling mechanism is constructed to focus the scattered light onto the active area of a single-photon counting module (SPCM, Thorlabs SPCM50A/M). To be specific, the scattered light is coupled to a step-index multimode fiber (LBTEK, MMC50L-0.22-PC-1) with a length of 1 m using a fiber collimator (LBTEK, FC520-6.1-PC). The light at the distal end of the fiber is collimated by another fiber collimator (LBTEK, FC520-6.1-PC) and is focused onto the SPCM via an aspheric lens.

Varied water turbidities are studied in optical experiments. The photon counts measured when using 5, 10, and 15-ml skimmed milk are shown in Figs. 3(a), 3(c), and 3(e), respectively. The dynamic and complex scattering in the water tank causes severe wavefront distortions. As can be seen in Figs. 3(a), 3(c), and 3(e), wave distortions manifest as time-varying scaling factors in the measured photon counts. To illustrate the scattering effect on the measured photon counts, histograms of the measured photon counts are shown in Figs. 4(a), 4(c), and 4(e). In theory, when there are no scattering media in the optical setup, the sequence of measured light intensities

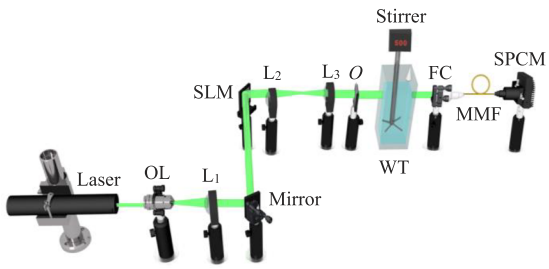

FIG. 2. A schematic experimental setup for the proposed photon-limited imaging through complex scattering media under low-light conditions. OL: objective lens; L_1: a collimation lens; L_2 and L_3: lenses to construct a 4*f* system; *O*: object; WT: water tank; FC: fiber collimator; and MMF: multimode fiber. For the sake of brevity, a neutral density filter placed before the object is omitted.

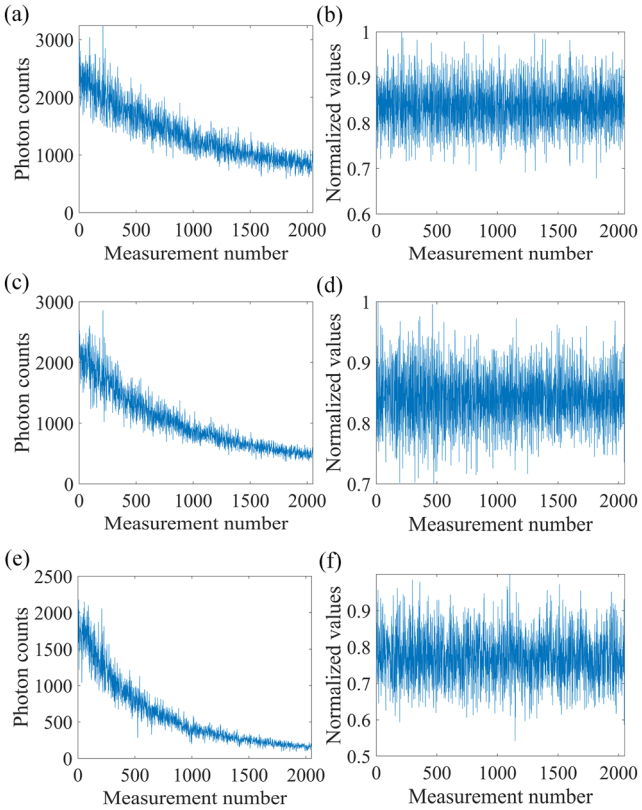

FIG. 3. (a), (c), and (e) Photon counts measured through dynamic and turbid water when 5, 10, and 15-ml skimmed milk is individually used in Fig. 2 and (b), (d), and (f) normalized data after applying the proposed correction method on the measured photon counts in (a), (c), and (e), respectively.

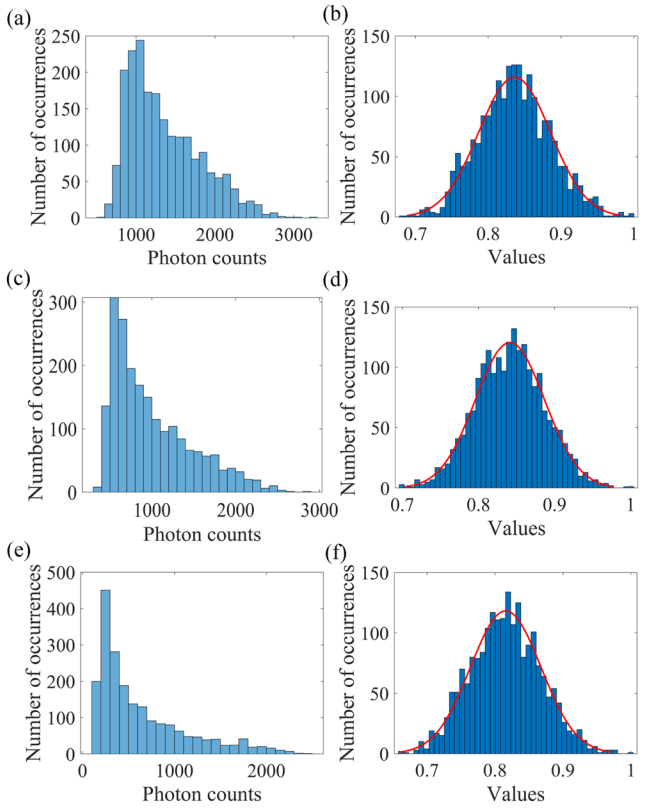

FIG. 4. (a), (c), and (e) Histograms of the measured photon counts in Figs. 3(a), 3(c), and 3(e) and (b), (d) and (f) histograms of the corrected data in Figs. 3(b), 3(d), and 3(f) with a fitting (indicated by the red curves).

in SPI should converge to a normal distribution.[41] As can be seen in Figs. 4(a), 4(c), and 4(e), the histograms exhibit a significant deviation from a normal distribution, and the deviation becomes more prominent as more skimmed milk is used. There is a scaling factor to generalize the distortion effect. The probability distribution of the collected single-pixel light intensities in complex media becomes non-Gaussian. It is well known that object reconstruction in SPI relies on a correlation between the illumination patterns and the measurements. However, the time-varying scaling factors induced by complex scattering in dynamic media obliterate the correlations carried in the measured photon counts, making it difficult to recover a high-quality object image.

Here, the proposed method is applied to eliminate the effects of time-varying scaling factors on the measured photons to restore the correlation property. The measurement correction results are shown in Figs. 3(b), 3(d), and 3(f). To verify the developed correction method, the histograms of corrected data in Figs. 3(b), 3(d), and 3(f) are shown in Figs. 4(b), 4(d), and 4(f). The shapes of the histograms closely match a normal distribution, showing a consistency with theories. The probability distributions of the corrected data are modeled via fitting a normal distribution, as indicated in Figs. 4(b), 4(d), and 4(f). It is demonstrated that the corrected data can align well with a theoretical model, showing high effectiveness of the proposed iterative algorithm for eliminating a series of time-varying scaling factors induced by complex scattering in dynamic media. Moreover, it is worth noting that the proposed iterative algorithm enforces algorithmic corrections on the distorted measurements without requiring any *prior* knowledge about scattering media. Therefore, the proposed method possesses high adaptability and can be applied in a wide range of scattering environments, such as dynamic smoke and random disturbance.

In the proposed iterative algorithm, a series of corrected measurements and an estimated object image can be obtained. These two outputs are fed to the designed URED engine for quality enhancement. Object reconstruction results are shown in Fig. 5, and the USAF 1951 resolution target (element 2 group 0) is used as an object. Here, the dimensions of a reconstructed object image are 64 × 64 pixels. For comparison, a conventional method, i.e., differential ghost imaging (DGI),[24] is also employed, and the reconstructed object images are shown in Figs. 5(a)–5(c) when 5, 10, and 15-ml skimmed milk is used, respectively. Effective information about the object cannot be observed in the reconstructed object images, when DGI is used. It is demonstrated that conventional methods could not work in complex environments under photon-limited conditions as the correlation property is broken by the time-varying

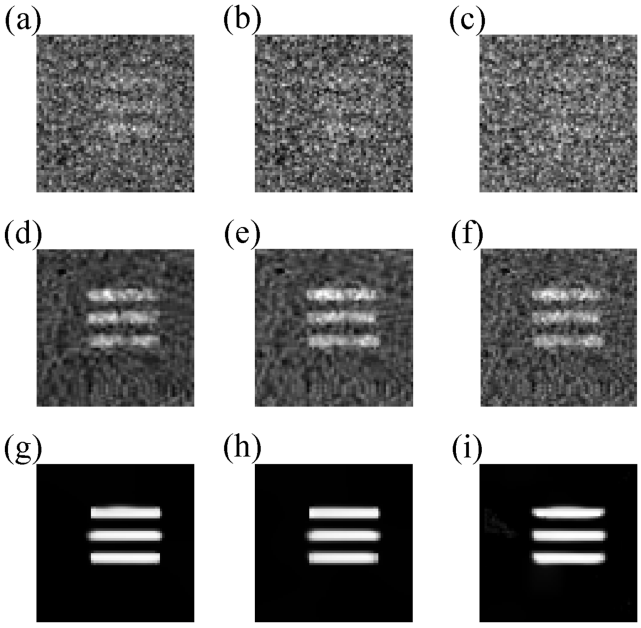

FIG. 5. Reconstructed object images obtained when 5, 10, and 15-ml skimmed milk is used in experiments. (a)–(c) Reconstructed object images using DGI, (d)–(f) reconstructions obtained by using the proposed iterative algorithm, and (g)–(i) reconstructed object images obtained after applying the URED, respectively, on those in (d)–(f).

scaling factors induced by complex scattering in dynamic media. The reconstructed object images obtained by using the proposed iterative algorithm are shown in Figs. 5(d)–5(f). The final reconstructions obtained by feeding the images in Figs. 5(d)–5(f) to the URED are shown in Figs. 5(g)–5(i), respectively. A spatial resolution of 890.9 μm is achieved in the proposed method. The experimental results exhibit high-quality object features, and high effectiveness and high robustness of the proposed method are validated.

To quantitatively evaluate the reconstruction quality, contrast-to-noise ratio (CNR)[42,43] is calculated, as described by

$$\mathrm{CNR} = \frac{\langle I_s \rangle - \langle I_b \rangle}{(\sigma_s + \sigma_b)/2}, \tag{10}$$

where $\langle I_s \rangle$ and $\langle I_b \rangle$, respectively, denote an average intensity of the signal region and background region (indicated in an inset in Fig. 6) in a reconstructed object image and σ_s and σ_b denote the standard deviations. The CNRs of the reconstructed object images using DGI in Figs. 5(a)–5(c) are 1.31, 0.94, and 0.70, showing low-quality object reconstruction. CNRs of the object images reconstructed by using the proposed iterative algorithm are 3.57, 3.71, and 3.11, as shown in Figs. 5(d)–5(f), respectively. CNRs of the object images are 25.91, 23.60, and 23.34 in Figs. 5(g)–5(i), respectively. The experiments demonstrate that object reconstruction with a high CNR can be implemented by using the proposed method.

Figure 6 shows the variations of CNRs of the reconstructed object images using DGI and the proposed method when the volumes of skimmed milk ranging from 0 to 18 ml are individually used in experiments. The speed of the stirrer is fixed at 500 rpm. High

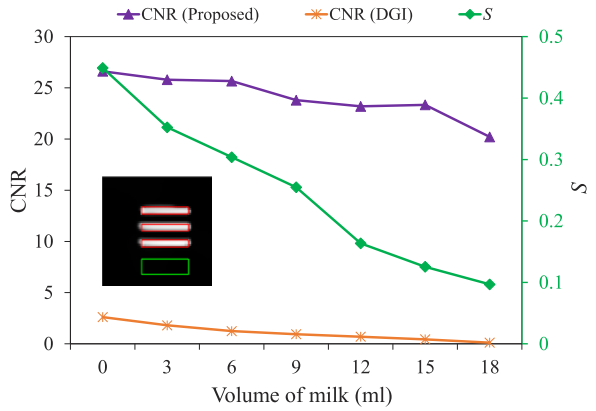

FIG. 6. Variation of CNRs of the reconstructed object images and the variance of S when different volumes of skimmed milk are individually used in experiments. For the CNR calculations, the signal region is indicated by the red boxes in the inset, and the background region is indicated by a green box. Parameter S denotes the photons of a 2D pattern per pixel.

CNRs can always be achieved in the proposed method. As the volume of skimmed milk increases, the CNRs show a slight decrease, verifying the high robustness of the proposed method. In contrast, the CNRs are low and could decrease to be zero at high milk volumes using DGI, showing vulnerability to the variations of water turbidity. It is worth noting that although the rotational speed of the stirrer is also a variable in experiments, which contributes to scattering media, it does not have much effect on the imaging quality.[44,45]

The proposed method is applied to further test other objects (i.e., "4," "T," "rectangle" and "51"). Figures 7(a)–7(d) show the reconstructed object images obtained by using DGI. The performance of DGI is significantly degraded by the presence of dynamic and complex scattering media, and object information cannot be clearly rendered. As the proposed method is applied, clear features about the objects can be retrieved and observed, as shown in Figs. 7(e)–7(h). It is demonstrated again that the proposed method can be applied to overcome the challenge induced by complex scattering in dynamic media under photon-limited conditions, and high-quality object images can always be recovered.

All experimental results aforementioned are obtained through complex scattering media at low-light levels. Here, the low-light condition is constructed using two ways. A neutral density filter is placed before the object with a high attenuation factor to control optical power. In addition, particles within scattering media also absorb the energy of the laser beam. An evaluation parameter S,[46,47] called the photons of a 2D pattern per pixel, is used to quantitatively describe low-light levels as defined by

$$S = \frac{1}{M}\sum_{i=1}^{M}\frac{\widehat{B}_i}{Y}, \tag{11}$$

where Y denotes the dimension of a reconstructed object image, i.e., 64 × 64 pixels in this study. The calculated values S are 0.44, 0.35, 0.33, 0.30, 0.25, 0.24, 0.16, 0.12, and 0.096 when 0, 3, 5, 6, 9, 10, 12, 15, and 18 ml skimmed milk is, respectively, used, as shown in Fig. 2. The calculated values S are 0.21, 0.34, 0.29, and 0.26 for the

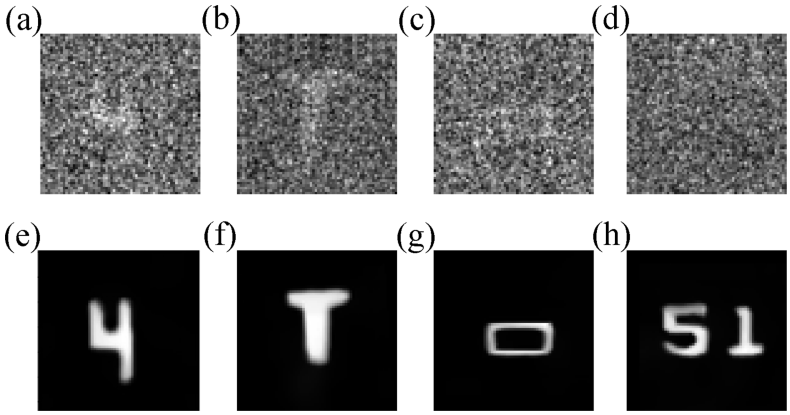

FIG. 7. Experimentally reconstructed object images (objects "4," "T," "rectangle," and "51") through dynamic and turbid water when 10 ml skimmed milk and a stirring speed of 500 rpm are used in Fig. 2. (a)–(d) Reconstructed object images obtained by using DGI and (e)–(h) reconstructed object images obtained by using the proposed method.

four objects shown in Fig. 7, respectively. It is verified that our experiments are conducted under low-light conditions. At these low-light levels, the proposed method can still be applied to recover high-quality object images, as shown in Figs. 5–7. The variation of S, when the volumes of skimmed milk ranging from 0 to 18 ml are individually used, is shown in Fig. 6. As a higher volume of skimmed milk is used, the value S decreases rapidly and the CNRs of the reconstructed object images show a slight decrease. It is illustrated that the proposed method is robust at different limited-photon levels.

IV. CONCLUSION

We have reported high-quality photon-limited imaging with a single-photon detector in dynamic and complex scattering environments. The proposed method adopts a designed iterative operation to implement effective corrections on the series of distorted measurements to generate corrected data and estimate an object image, which are further fed to the URED for quality enhancement. A series of optical experiments have been conducted to verify feasibility and effectiveness of the proposed method in complex scenarios. Experimental results demonstrate that the proposed method can always be applied to effectively eliminate the series of dynamic scaling factors and reconstruct high-quality object images in complex scattering environments at low-light levels. The proposed method opens up an avenue for the applications of single-photon detection techniques in real-world scenarios, e.g., complex scattering in dynamic media.

ACKNOWLEDGMENTS

This work was supported by the Hong Kong Research Grants Council General Research Fund (Nos. 15224921, 15223522, and 15237924), the Hong Kong Research Grants Council Collaborative Research Fund (No. C5047-24G), the Guangdong Basic and Applied Basic Research Foundation (No. 2025A1515011411), and the Hong Kong Polytechnic University (No. 1-CDJA, 1-WZ4M).

AUTHOR DECLARATIONS

Conflict of Interest

The authors have no conflicts to disclose.

Author Contributions

Yining Hao: Data curation (lead); Formal analysis (lead); Investigation (lead); Methodology (lead); Writing – original draft (lead). **Yang Peng**: Formal analysis (lead); Investigation (lead). **Tianshun Zhang**: Formal analysis (lead); Investigation (lead). **Wen Chen**: Conceptualization (lead); Formal analysis (lead); Funding acquisition (lead); Methodology (lead); Project administration (lead); Resources (lead); Supervision (lead); Writing – review & editing (lead).

DATA AVAILABILITY

The data that support the findings of this study are available from the corresponding author upon reasonable request.

REFERENCES

[1] G. C. Holst, *CCD Arrays, Cameras and Displays*, 2nd ed. (SPIE Press, Bellingham WA, 1998).
[2] Y. Chen, J. D. Müller, P. T. C. So, and E. Gratton, "The photon counting histogram in fluorescence fluctuation spectroscopy," Biophys. J. **77**, 553–567 (1999).
[3] A. McCarthy, R. J. Collins, N. J. Krichel, V. Fernández, A. M. Wallace, and G. S. Buller, "Long-range time-of-flight scanning sensor based on high-speed time-correlated single-photon counting," Appl. Opt. **48**, 6241–6251 (2009).
[4] W. Becker, *Advanced Time-Correlated Single Photon Counting Techniques*, 1st ed. (Springer, 2005).
[5] A. Migdall, "Introduction to journal of modern optics special issue on single-photon: Detectors, applications, and measurement methods," J. Mod. Opt. **51**, 1265–1266 (2004).
[6] R. H. Hadfield, "Single-photon detectors for optical quantum information applications," Nat. Photonics **3**, 696–705 (2009).
[7] M. Ghioni, A. Gulinatti, I. Rech, F. Zappa, and S. Cova, "Progress in silicon single-photon avalanche diodes," IEEE J. Sel. Top. Quantum Electron. **13**, 852–862 (2007).
[8] C. Bruschini, H. Homulle, I. M. Antolovic, S. Burri, and E. Charbon, "Single-photon avalanche diode imagers in biophotonics: Review and outlook," Light: Sci. Appl. **8**, 87 (2019).
[9] Y. Yang, J. Shi, F. Cao, J. Peng, and G. Zeng, "Computational imaging based on time-correlated single-photon-counting technique at low light level," Appl. Opt. **54**, 9277–9283 (2015).
[10] D. Shin, F. Xu, D. Venkatraman, R. Lussana, F. Villa, F. Zappa, V. K. Goyal, F. N. C. Wong, and J. H. Shapiro, "Photon-efficient imaging with a single-photon camera," Nat. Commun. **7**, 12046 (2016).

[11] D. Shin, A. Kirmani, V. K. Goyal, and J. H. Shapiro, "Photon-efficient computational 3-D and reflectivity imaging with single-photon detectors," IEEE Trans. Comput. Imaging **1**, 112–125 (2015).
[12] Y. Wang, K. Huang, J. Fang, M. Yan, E. Wu, and H. Zeng, "Mid-infrared single-pixel imaging at the single-photon level," Nat. Commun. **14**, 1073 (2023).
[13] K. Song, Y. Bian, F. Zeng, Z. Liu, S. Han, J. Li, J. Tian, K. Li, X. Shi, and L. Xiao, "Photon-level single-pixel 3D tomography with masked attention network," Opt. Express **32**, 4387–4399 (2024).
[14] X. Liu, J. Shi, L. Sun, Y. Li, J. Fan, and G. Zeng, "Photon-limited single-pixel imaging," Opt. Express **28**, 8132–8144 (2020).
[15] I. M. Vellekoop and A. P. Mosk, "Focusing coherent light through opaque strongly scattering media," Opt. Lett. **32**, 2309–2311 (2007).
[16] I. M. Vellekoop, A. Lagendijk, and A. P. Mosk, "Exploiting disorder for perfect focusing," Nat. Photonics **4**, 320–322 (2010).
[17] I. M. Vellekoop, "Feedback-based wavefront shaping," Opt. Express **23**, 12189–12206 (2015).
[18] Z. Yaqoob, D. Psaltis, M. S. Feld, and C. Yang, "Optical phase conjugation for turbidity suppression in biological samples," Nat. Photonics **2**, 110–115 (2008).
[19] S. M. Popoff, G. Lerosey, R. Carminati, M. Fink, A. C. Boccara, and S. Gigan, "Measuring the transmission matrix in optics: An approach to the study and control of light propagation in disordered media," Phys. Rev. Lett. **104**, 100601 (2010).
[20] M. Kim, W. Choi, Y. Choi, C. Yoon, and W. Choi, "Transmission matrix of a scattering medium and its applications in biophotonics," Opt. Express **23**, 12648–12668 (2015).
[21] I. Freund, M. Rosenbluh, and S. Feng, "Memory effects in propagation of optical waves through disordered media," Phys. Rev. Lett. **61**, 2328–2331 (1988).
[22] M. P. Edgar, G. M. Gibson, and M. J. Padgett, "Principles and prospects for single-pixel imaging," Nat. Photonics **13**, 13–20 (2019).
[23] J. H. Shapiro, "Computational ghost imaging," Phys. Rev. A **78**, 061802 (2008).
[24] F. Ferri, D. Magatti, L. A. Lugiato, and A. Gatti, "Differential ghost imaging," Phys. Rev. Lett. **104**, 253603 (2010).
[25] Z. Zhang, X. Ma, and J. Zhong, "Single-pixel imaging by means of Fourier spectrum acquisition," Nat. Commun. **6**, 6225 (2015).
[26] Z. Zhang, X. Wang, G. Zheng, and J. Zhong, "Hadamard single-pixel imaging versus Fourier single-pixel imaging," Opt. Express **25**, 19619–19639 (2017).
[27] M. Bina, D. Magatti, M. Molteni, A. Gatti, L. A. Lugiato, and F. Ferri, "Backscattering differential ghost imaging in turbid media," Phys. Rev. Lett. **110**, 083901 (2013).
[28] L. Zhou, Y. Xiao, and W. Chen, "High-resolution self-corrected single-pixel imaging through dynamic and complex scattering media," Opt. Express **31**, 23027–23039 (2023).
[29] Y. Hao, Y. Xiao, and W. Chen, "Single-pixel imaging through random media with automated adaptive corrections," Appl. Phys. Lett. **126**, 131105 (2025).
[30] M. F. Duarte, M. A. Davenport, D. Takhar, J. N. Laska, T. Sun, K. F. Kelly, and R. G. Baraniuk, "Single-pixel imaging via compressive sampling," IEEE Signal Process. Mag. **25**, 83–91 (2008).
[31] W. L. Chan, K. Charan, D. Takhar, K. F. Kelly, R. G. Baraniuk, and D. M. Mittleman, "A single-pixel terahertz imaging system based on compressed sensing," Appl. Phys. Lett. **93**, 121105 (2008).
[32] F. Li, M. Zhao, Z. Tian, F. Willomitzer, and O. Cossairt, "Compressive ghost imaging through scattering media with deep learning," Opt. Express **28**, 17395–17408 (2020).
[33] F. Wang, C. Wang, C. Deng, S. Han, and G. Situ, "Single-pixel imaging using physics enhanced deep learning," Photonics Res. **10**, 104–110 (2022).
[34] Y. Peng and W. Chen, "Deep learning-enhanced ghost imaging through dynamic and complex scattering media with supervised corrections of dynamic scaling factors," Appl. Phys. Lett. **124**, 181104 (2024).
[35] H. Liu, K. Song, Y. Bian, and L. Xiao, "Single-photon single-pixel dual-wavelength imaging via frequency spectral harmonics extraction strategy," Opt. Express **33**, 1636–1646 (2025).
[36] J. R. Fienup, "Phase retrieval algorithms: A comparison," Appl. Opt. **21**, 2758–2769 (1982).
[37] B. Ergen, "Signal and image denoising using wavelet transform," in *Advances in Wavelet Theory and Their Applications in Engineering, Physics and Technology* (InTech, 2012), pp. 495–514.
[38] S. Boyd, N. Parikh, E. Chu, B. Peleato, and J. Eckstein, "Distributed optimization and statistical learning via the alternating direction method of multipliers," Found. Trends Mach. Learn. **3**, 1–122 (2011).
[39] A. Buades, B. Coll, and J. M. Morel, "A non-local algorithm for image denoising," in *IEEE Computer Society Conference on Computer Vision and Pattern Recognition* (IEEE, 2005), Vol. 2, pp. 60–65.
[40] L. Chen, X. Chu, X. Zhang, and J. Sun, "Simple baselines for image restoration," in *European Conference on Computer Vision* (Springer, 2022), Vol. 13667, pp. 17–33.
[41] J. Leng, W.-K. Yu, and S.-F. Wang, "Formation mechanism of correspondence imaging with thermal light," Phys. Rev. A **101**, 033835 (2020).
[42] B. Redding, M. A. Choma, and H. Cao, "Speckle-free laser imaging using random laser illumination," Nat. Photonics **6**, 355–359 (2012).
[43] Y. Peng and W. Chen, "Learning-based correction with Gaussian constraints for ghost imaging through dynamic scattering media," Opt. Lett. **48**, 4480–4483 (2023).
[44] Q. Song, Q. H. Liu, and W. Chen, "High-resolution ghost imaging through dynamic and complex scattering media with adaptive moving average correction," Appl. Phys. Lett. **124**, 211104 (2024).
[45] Z. Xu, Q. Song, and W. Chen, "High-fidelity correspondence imaging in complex media with varying thresholds and 1-bit compressive sensing," Appl. Phys. Lett. **124**, 111105 (2024).
[46] J.-Z. Yang, M.-F. Li, X.-X. Chen, W.-K. Yu, and A.-N. Zhang, "Single-photon quantum imaging via single-photon illumination," Appl. Phys. Lett. **117**, 214001 (2020).
[47] F. Zeng, Y. Bian, K. Song, H. Liu, S. Zhao, X. Wang, F. Zhang, H. Ge, D. Wang, and L. Xiao, "Photon-level single-pixel wavefront imaging through turbid underwater environment," APL Photonics **10**, 060805 (2025).